3078–3093 *Nucleic Acids Research, 2023, Vol. 51, No. 7* *Published online 2 February 2023*
https://doi.org/10.1093/nar/gkad061

DIS3L2 ribonuclease degrades terminal-uridylated RNA to ensure oocyte maturation and female fertility

Di Wu, Monique Pedroza, Jonathan Chang and Jurrien Dean*

Laboratory of Cellular and Developmental Biology, NIDDK, National Institutes of Health, Bethesda, MD 20892, USA

Received August 03, 2022; Revised January 03, 2023; Editorial Decision January 16, 2023; Accepted January 20, 2023

ABSTRACT

During oocyte development in mice, transcripts accumulate in the growth phase and are subsequently degraded during maturation. At the transition point between growth and maturation, oocytes have an intact nucleus or germinal vesicle (GV), and terminal uridylation labels RNA for degradation in meiosis I. By profiling the transcriptome using single-oocyte long-read PacBio RNA sequencing, we document that a small cohort of mRNAs are polyadenylated after terminal uridylation in GV oocytes [designated uridylated-poly(A) RNA]. Because DIS3L2 ribonuclease is known to degrade uridylated transcripts, we established oocyte-specific *Dis3l2* knockout mice (*Dis3l2*^{cKO}). Upon DIS3L2 depletion, uridylated-poly(A) RNAs remain intact which increases their abundance, and they predominate in the transcriptome of *Dis3l2*^{cKO} oocytes. The abundance of uridylated-poly(A) RNA in *Dis3l2*^{cKO} oocytes arises not only from insufficient degradation, but also from the stabilizing effect of subsequent polyadenylation. Uridylated-poly(A) RNAs have shorter poly(A) tails and their translation activity decreases in *Dis3l2*^{cKO} oocytes. Almost all *Dis3l2*^{cKO} oocytes arrest at the GV stage, and female mice are infertile. Our study demonstrates multiple fates for RNA after terminal uridylation and highlights the role of DIS3L2 ribonuclease in safeguarding the transcriptome and ensuring female fertility.

INTRODUCTION

The maternal transcriptome is sculpted by active transcription and degradation to ensure a pool of RNA required for fertility and early embryonic development. At birth, female mice have their complete complement of germ cells (~20 μm diameter oocytes) which become surrounded by a single layer of squamous granulosa (somatic) cells to form primordial follicles. During a 2 week growth phase, genes are actively transcribed, and fully grown oocytes (~80 μm) arrest in prophase I of meiosis with an intact nucleus (germinal vesicle or GV). During growth, genes are robustly transcribed, and oocytes accumulate maternal RNA. In fully grown oocytes, activation of CDK1/cyclin B and the surge of luteinizing hormone trigger the release of GV oocytes from prophase I and permit progression through meiosis (1). During meiotic maturation, transcription is terminated and the oocyte transcriptome is shaped by RNA degradation to prepare for the maternal to zygotic transition (2). Disruption of RNA degradation can result in meiotic or embryonic arrest (3,4).

Multiple mechanisms of selective RNA destruction occur during oocyte maturation. We have previously reported that the RNA exosome complex targets various RNAs in GV oocytes for degradation or processing (4). In parallel with RNA exosome-mediated 3′ degradation, DIS3L2, a DIS3 homolog, functions as an RNA exosome-independent ribonuclease primarily in the cytoplasm (5,6). DIS3L2 preferentially degrades uridylated RNAs in somatic cells (6,7) and is reported to degrade let-7 precursor RNA following TUT4/TUT7-mediated oligo-uridylation (7,8). In somatic cells, inactivation of DIS3L2 results in cell division defects and overgrowth, which have been linked to congenital diseases including Perlman syndrome and Wilms tumor in humans (5,9). More recently, DIS3L2-mediated decay has been shown to protect endoplasmic reticulum-targeted mRNA translation, stem cell differentiation and intracellular calcium homeostasis (10).

The nucleotide composition of mRNA tails is dynamic due to polyadenylation and deadenylation which are tightly associated with RNA stability and translation into protein (11–13). In GV oocytes, the interplay between these two processes determines the composition of cytoplasmic RNA tails (3,14,15). While many dormant RNAs are recruited for polyadenylation and translation (3,16–19), others are deadenylated followed by TUT4/7-mediated oligo-uridylation which marks a subset for degradation (15).

*To whom correspondence should be addressed. Tel: +1 301 496 2738; Fax: +1 301 496 5239; Email: jurrien.dean@nih.gov
Present addresses:
Monique Pedroza, Department of Genetics, Yale School of Medicine, Yale University, New Haven, CT 06510, USA.
Jonathan Chang, Department of Stem Cell Biology and Regenerative Medicine, Keck School of Medicine, University of Southern California, Los Angeles, CA 90033, USA.

Because of the known TUT4/7–DIS3L2 pathway in miRNA processing, it is possible that TUT4/7-uridylated RNA in mouse oocytes will be degraded by DIS3L2. However, the genetic interaction of TUT4/7 and DIS3L2, and the precise role of DIS3L2 ribonuclease in determining the oocyte transcriptome remain incompletely understood.

A recently developed single-oocyte long transcript sequencing method, PAIso-seq [Poly(A) inclusive RNA isoform sequencing], provides a platform for profiling RNA tail dynamics (20). PAIso-seq captures and sequences entire RNA molecules from the poly(A) end, which precisely describes splicing isoforms and composition of post-transcriptional tails. In this study, we discovered the presence of uridylated-poly(A) RNA by mouse single-oocyte PAIso-seq. Uridylated-poly(A) RNA has a string of uridine nucleotides immediately following the 3′-untranslated region (UTR) which is added post-transcriptionally and is not a part of the poly(A) tail. The uridine stretch is followed by polyadenylation at the 3′ ends and is dramatically stabilized upon genetic depletion of DIS3L2 (*Dis3l2*^{cKO}). A combination of single-oocyte poly(A) RNA-seq and total RNA-seq documented global tail shortening and transcript accumulation in *Dis3l2*^{cKO} oocytes. In addition, we compare reporter RNAs with different tails and discover lower translation of uridylated-poly(A) RNA. Lastly, we investigate the relationship between *Tut4/7*^{cKO} and *Dis3l2*^{cKO} oocytes to explore genetic interactions. We determined that DIS3L2 ribonuclease not only targets TUT4/7-uridylated RNA, but also degrades uridylated-poly(A) RNA generated from deadenylated RNA undergoing tail editing. Rather than targeted degradation, our observations suggest more types of RNA tail editing in addition to adenylation, deadenylation and uridylation in mouse oocytes. The persistence of RNA and disrupted translation act synergistically to cause GV arrest of *Dis3l2*^{cKO} oocytes and female infertility.

MATERIALS AND METHODS

Establishment of *Dis3l2*$^{flox/flox}$ mice

Two loxP sites were inserted surrounding the second exon of the *Dis3l2* gene using CRISPR/Cas9 [clustered regularly interspaced short palindromic repeats (CRISPR)/CRISPR-associated peptide 9 (Cas9)]. Two guide RNAs (gRNAs) were synthesized by *in vitro* transcription using the MEGAshortscript™ T7 Transcription Kit (Thermo Fisher Scientific AM1354). The DNA templates for gRNA were synthesized as single-stranded DNA (ssDNA) by Integrated DNA Technologies (IDT). The ssDNA was amplified by polymerase chain reaction (PCR) into double-stranded DNA and purified. A 500 ng aliquot of purified DNA templates was used in each *in vitro* synthesis reaction, which also contained 2 μl of ATP, CTP, GTP and UTP, 2 μl of T7 10× reaction buffer and 2 μl of T7 enzyme mix. Reactions were incubated at 37°C for 2 h, treated by DNase and purified using the MEGAclear™ Kit (Thermo Fisher Scientific AM1908). Homology-directed repair templates for CRISPR/Cas9 were synthesized by IDT as ssDNA. Cas9 mRNA was synthesized by *in vitro* transcription using Addgene #42251 plasmid (21) and the mMESSAGE mMACHINE® T7 ULTRA Transcription Kit. Synthesized Cas9 mRNA was purified using the MEGAclear™ Kit. The injection mix contained two gRNAs (each 50 ng/μl), two homology-directed repair template DNAs (each 100 ng/μl) and Cas9 mRNA (100 ng/μl).

B6D2F$_1$ female mice were hormone stimulated for superovulation and mated with B6D2F$_1$ males. Embryos were collected in M2 medium (CytoSpring M2114). Cumulus cells were removed with hyaluronidase-M2 medium (CytoSpring M2111HV) at 37°C for 1–2 min. Embryos were washed with M2 medium 10 times and cultured in KSOM (CytoSpring K0114) at 37°C, 5% CO_2 for 5 h prior to microinjection. Embryos after microinjection were cultured in KSOM at 37°C, 5% CO_2 overnight. The microinjection protocol and settings were the same as previously described (4). Embryos were transferred into the oviducts of pseudopregnant ICR-CD1 females 0.5 days post-coitus.

After pups (F$_0$) were born, the DNA from each loxP site was amplified and commercially sequenced at Genewiz. Mice having both loxP sites were crossed with B6D2F$_1$ males for F$_1$ mice. F$_1$ mice with both loxP sites confirmed by DNA sequence were crossed with *Zp3-cre* mice (22). All DNA oligos for microinjection, *in vitro* transcription and genotyping PCR are listed in Supplementary Table S5.

Oocyte collection and *ex vivo* culture

Ovaries (6 weeks to 4 months) were dissected into phosphate-buffered saline (PBS) and the surrounding lipid and tissue were removed. Ovaries were washed with M2 medium and punctured using a 30 gauge needle. Oocytes were collected in M2 medium and cultured at 37°C, 5% CO_2 for 3, 6 and 16 h.

Single-oocyte RNA-seq and analysis

Both poly(A) RNA-seq and total RNA after rRNA depletion (RiboMinus) RNA-seq were performed as previously described (4). Briefly, for poly(A) RNA-seq, oocytes were collected individually in 2.5 μl of RLT plus (Qiagen). A 1 μl aliquot of 1:10^5-diluted ERCC RNA Spike-In Mix (External RNA Controls Consortium) was added to each oocyte lysate. Poly(A) RNA was enriched by oligo(dT) beads and reverse transcribed. cDNA was amplified and purified for library construction using the Nextera XT kit. RiboMinus RNA-seq was performed using the Ovation Solo kit.

When processing sequencing data, original FASTQ files were mapped to mm10 using STAR (2.7.8a) (23). BAM files were counted using HTSeq (0.11.4) (24). Differential analysis was performed using DESeq2 (25). Libraries were normalized using ERCC molecules. All RNA-seq analysis codes are available at https://github.com/Di-aswater/public-dis3l2-analysis. Raw and processed files are in GSE208531.

Single-oocyte PAIso-seq

Single-oocyte PAIso-seq was performed (20) using a protocol kindly shared by Dr Yusheng Liu from the Institute of Genetics and Developmental Biology, Chinese Academy of Sciences, with minor modifications. Oocytes at the GV

stage were washed using 1% bovine serum albumin (BSA)–PBS three times and collected individually into 11 μl of newly prepared lysis buffer. The lysis buffer contained 0.5 μl of SUPERase• In™ RNase Inhibitor (20 U/μl) (Thermo Fisher Scientific AM2696) and 10 μl of 0.2% Triton X-100 in PBS. Oocyte lysate was stored at –80°C until use.

Poly(A) spike-in molecules were the purified PCR products of the *mCherry* cDNA with 10 adenosines (10A), 30A, 50A, 70A and 100A at the 3′ end. Each spike-in molecule was barcoded and purified. Spike-in molecules (20 ng/μl) were mixed equally and stored at –20°C. The poly(A) mixture was added to each sample in a 1:1000 mass ratio.

Oocyte lysates were heated at 80°C for 5 min. Each oocyte was barcoded at the end extension step with differently indexed dU-containing DNA templates. In each 12 μl oocyte lysate, 1 μl of end extension oligo (50 μM) was added and the reaction was incubated at 80°C for 5 min, and 37°C for 10 min to anneal the end extension oligo to the poly(A) of RNA. After annealing, 1 μl of dithiothreitol (DTT; 100 μM, SuperScript™ II Reverse Transcriptase kit, Thermo Fisher 18064014), 4 μl of Superscript II first-strand buffer (5×), 1 μl of dNTP mix (Thermo Fisher 18427013), 0.5 μl of SUPERase• In™ RNase Inhibitor (20 U/μl) (Thermo Fisher AM2696), 1 μl of Klenow fragment (3′→5′ exo-) (NEB M0212S) and 0.5 μl of nuclease-free water were added to each reaction. Oocyte lysates were incubated at 37°C for 1 h and at 80°C for 10 min. A 1 μl aliquot of USER enzyme (NEB M5505S) was added to each reaction and incubated at 37°C for 30 min to digest the end-extension oligos. RNA from each reaction was purified using the NucleoSpin RNA XS Micro kit (Takara 740902.50). Each sample was eluted using 15 μl of nuclease-free water.

A 7 μl aliquot of the above purified end-extended RNA was used for reverse transcription and template switching. In each reaction, there was 7 μl of RNA, 0.4 μl of RT primer and 1 μl of dNTP. The reaction was incubated at 72°C for 3 min and put on ice immediately. Then 1 μl of SuperScript II reverse transcriptase (200 U/μl) (Thermo Fisher 18064014), 0.5 μl of RNase Inhibitor (Thermo Fisher AM2696), 4 μl of Superscript II first-strand buffer (5×), 1 μl of DTT, 4 μl of Betaine (5 M) (Sigma Aldrich B0300-1VL), 0.12 μl of $MgCl_2$ (1 M), 0.2 μl of template switch oligo and 0.78 μl of nuclease-free water were added to each reaction. Reactions were incubated at 42°C for 90 min, 10 cycles of 50°C for 2 min followed by 42°C for 2 min and 70°C for 15 min. Reactions were then amplified by PCR for 26 cycles. In each PCR, there was 20 μl of reverse transcription product, 25 μl of KAPA HiFi HotStart ReadyMix (2×) (KAPA Biosystems KK2601) and 5 μl of PCR primer. The PCR was purified using AMPure XP beads (Beckman Coulter A63881). cDNA samples were then processed at the NIH Intramural Sequencing Center (NISC) for PacBio sequencing library preparation and PacBio sequencing. Samples were run on 2 SMRTCells and sequenced on Sequel II (25 h collection time).

Single-oocyte PAIso-seq analysis

Subreads were converted into circular consensus sequences (CCSs) by number of passes ≥10. The CCS-LIMA barcode detection process was run to mark the reads for the presence of barcodes. The IsoSeq Refine step was run to find full-length non-chimeric (FLNC) reads classified by: (i) the presence of 5′ and 3′ primer sequences on ends; (ii) the correct orientation of the 5′ and 3′ barcode sequences; and (iii) the presence of poly(A); the chimeric sequences with the barcode in the middle were removed. Fastq read and poly(A) length were processed (20). For mapping analysis, the sam files were processed using the id_features_pandas.py file using Mus_Musculus.GRCm38.102.gtf as the reference (details in mapping.ipynb). The 3′-unmapped region was extracted utilizing get_sam_tails.py using all the sam files as the input. The length of the unmapped region of each transcript was recorded as cigar_S_len (details in get_sam_unmapped_tails.ipynb). The poly(A) of the transcripts was measured as described (20). Briefly, at the 3′ terminus, the poly(A) sequence contained at least five continuous adenosines, and the percentage of the non-A residues was <50% and the number of non-A residues was <20. The summarized information for all transcripts of all libraries is in the PAIsoSeq_Wu_2022.csv file under GSE208531. PAIso-seq analysis and figure preparation codes are available at https://github.com/Di-aswater/public-dis3l2-analysis.

When defining poly(A) RNA and uridylated-poly(A) RNA, the length of the 3′-unmapped region was compared with the length of poly(A). When the length of the 3′-unmapped region was less than or equal to the length of the poly(A), the two regions were mostly identical with only subtle mixed base additions (MBAs) due to imprecisely assigning the few adenosines to the coding region or to the poly(A) region. Thus, the MBA regions were mostly short and located in the poly(A) region. On the other hand, when the 3′-unmapped region was larger than the poly(A), the length of the MBA regions was significantly longer, contained a higher percentage of uridine than adenosine and were isolated regions between the coding region and poly(A). This group of RNAs was designated uridylated-poly(A) or U-poly(A) RNA.

Polyadenylation site mapping was performed using TAPAS (26) with a read length of 500 which was the peak value of the read length distribution. Read coverage of individual sequence files was obtained using Samtools. The plot of read coverage was performed using deepTools (27).

Ovary section, staining and imaging

Ovary section and staining were performed as previously described (4). Briefly, ovaries were dissected into PBS, washed and fixed using newly prepared 2.5% glutaraldehyde (diluted from VWR 100504-790), 2.5% paraformaldehyde (diluted from Fisher Scientific 50–980-492) in 0.083 M sodium cacodylate buffer (VWR 102090–966) for 5 h at 4°C. Ovaries were washed with 0.083 M sodium cacodylate buffer and kept at 4°C overnight. Ovaries were transferred into 70% ethanol and stored at 4°C. Periodic acid–Schiff (PAS) staining and mounting were performed by American Histo Labs. Every 20th section (2 μm) was selected for imaging with a Zeiss Lab.A1 Axio microscope. Images tiles were assembled using Fiji software.

HPG translation labeling

Homopropargylglycine (HPG) translation labeling was performed using the Click-iT® HPG Alexa Fluor® 594 Protein Synthesis Assay Kit. Briefly, GV oocytes were collected in M2 (2.5 μM milrinone) medium. Oocytes were cultured in M2 (2.5 μM milrinone) medium containing HPG (50 μM) for 30 min at 37°C. Oocytes were washed twice with PBS and fixed in 2% paraformaldehyde for 30 min at room temperature. Oocytes were washed with 3% BSA–PBS buffer twice and treated with 0.5% Triton X-100 for 20 min at room temperature. Oocytes were washed with 3% BSA–PBS twice. Oocytes were transferred into Click-iT reaction cocktail and incubated for 30 min at room temperature. Oocytes were washed with Component F, washed twice with PBS and stained with Hoechst for 15 min at room temperature. Oocytes were imaged using an LSM 780 confocal microscope (Carl Zeiss).

mRNA synthesis for microinjection

mRNA was *in vitro* synthesized using a mMESSAGE mMACHINE® T7 ULTRA Transcription Kit (Thermo Fisher Scientific AM1345). mVenus DNA template was from pcDNA4-TO-mVenus-MAP-Puro (Addgene #44118). The tail of the mVenus DNA was modified using the NEB Gibson Assembly® method. An XbaI enzyme site was placed immediately after the edited tail to linearize the DNA template. During *in vitro* transcription, one reaction contained 10 μl of 2× NTP/ARCA buffer, 2 μl of 10× T7 reaction buffer, 500 ng of DNA and 2 μl of T7 enzyme in a 20 μl system. The reaction was incubated at 37°C for 2 h. DNA was digested using 1 μl of TURBO DNases by incubation at 37°C for 15 min. RNA not for polyadenylation was directly purified. RNA for polyadenylation was processed for the poly(A) tailing. For each 20 μl *in vitro* transcription reaction, 36 μl of nuclease-free water, 20 μl of 5× E-PAP buffer, 10 μl of $MnCl_2$, 10 μl of ATP and 4 μl of E-PAP were added. The reaction was incubated at 37°C for 30 min and purified using the MEGAclear™ Kit (Thermo Fisher Scientific AM1908).

mRNAs of tail-edited *mVenus* and *mCherry* were synthesized as described above. The synthesized tail regions are listed in Supplementary Table S5. Each of the mVenus-derived mRNAs was mixed with *mCherry* mRNA at a final concentration of 160 ng/μl. The microinjection system was composed of a microscope (Zeiss Axiovert S100 inverted scope), two micro manipulators (Eppendorf Transferman NK2) and an injector (Eppendorf Femtojet 4i). During injection, the injector was set to 'auto', the injection time was set to 0.1 s, the compensation pressure was set to 15 hPa and the injection pressure was set to 300–500 hPa. The holding pipet was an Eppendorf VacuTip I (Eppendorf 5195000036). The needle was prepared from borosilicate glass with filament (BF150-75-10) using a Sutter Flaming/Brown Micropipette Puller. Injection samples were loaded into the needle from the end using an Eppendorf loading pipet Microloader (Eppendorf 930001007).

During microinjection, GV oocytes were in M2 medium (2.5 μM milrinone) on a glass slide. After injection, oocytes were washed with M2 medium (2.5 μM milrinone) and cultured at 37°C for 2 h until collection.

Quantitative PCR to detect the level of injected mRNAs

GV oocytes after microinjection were collected into 350 μl of RLT plus (Qiagen) and frozen at –80 C until all groups of oocytes were collected. Total RNA of each sample was extracted using the Qiagen RNeasy Plus Micro Kit (Qiagen 74034). Three methods were used for reverse transcription with SuperScript™ III First-Strand Synthesis Super Mix (Invitrogen 18080400). For the oligo(dT) method, reverse transcription was primed by the oligo(dT) primer. For the random-primer method, random hexamers were used. For the GSP-1 and GSP-2 methods, before reverse transcription, tail ligation of adaptors was performed. In a 20 μl reaction, there were 2 μl of 1× T4 RNA ligase reaction buffer (NEB M0204S), 6 μl of 15–25% (w/v) polyethylene glycol (PEG) 8000, 0.5 μl of RNase Inhibitor, 1 μl of T4 RNA ligase, 2 μl of 1 mM ATP, 0.5 μl of adaptor oligo (5′-P-GGTCACCTTGATCTGAAGC-NH2-3′, 100 μM), 0.5 μl of nuclease-free water and 6 μl of total RNA from the above extraction plus 500 ng of carrier RNA (Qiagen 74034). The reaction was incubated at 25°C for 3 h and then heat inactivated by 65°C for 15 min. The tail adaptor-ligated total RNA was then used for reverse transcription. The oligo (P2-A/Tmix: 5′-GCTTCAGATCAAGGTGACCWWWWW-3′) was used as the primer for reverse transcription. The PCR oligonucleotides are listed in Supplementary Table S5.

Quantitative PCR (qPCR) was performed in a 10 μl reaction system with three technical replicates and 2–3 biological replicates. qPCR was carried out by iTaq Universal SYBR Green Supermix (Bio-Rad 1725121) and QuantStudio 6 Flex Real-Time PCR System (Thermo Fisher Scientific).

Immunostaining and antibodies

Oocytes were collected and fixed using 2% paraformaldehyde at 37°C for 30 min. Oocytes were washed twice with PBS–3% polyvinylpyrrolidone-40 and 0.1% Tween-20 (PBVT) and permeabilized using 0.5% Triton X-100 PBS for 30 min at room temperature. Oocytes were washed once with PBVT and incubated in blocking buffer (5% normal goat serum–PBVT, Sigma G9023-10ML) for 30 min at room temperature. Oocytes were incubated in primary antibody diluted in blocking buffer overnight at 4°C. On the second day, oocytes were washed three times for 30 min at room temperature using PBVT and incubated in secondary antibody overnight at 4°C. On the third day, oocytes were washed three times for 30 min at room temperature using PBVT and stained with Hoechst (1:5000 dilution from 10 mg/ml in PBVT) for confocal imaging (LSM 780, Carl Zeiss). The antibodies used and their dilution were: WEE1, 1:200 (Proteintech 29474–1-AP); pCDK1 (Thr14, Tyr15), 1:200 (ThermoFisher 701808); and goat anti-rabbit IgG (H + L) cross-adsorbed secondary antibody, 1:500 (Alexa Fluor 546, Invitrogen A-11010).

Statistical analyses

The sample sizes for each experiment are given in the figures. The methods of group comparison and statistical analyses are also described in each figure legend.

Ethics approval and consent to participate

Mice were maintained and handled in compliance with the guidelines of the Animal Care and Use Committee of the National Institutes of Health (NIDDK animal study protocol K018LCDB21).

RESULTS

Uridylated-poly(A) transcripts are present in mouse GV-intact oocytes

Using single-oocyte PAIso-seq (20) of 10 GV (germinal vesicle-intact) oocytes from two mice, we obtained 151 723 CCS (circular consensus sequence) reads that were assigned to 9351 genes. Five or more transcripts were detected for ∼60% of these genes (Supplementary Figure S1A) and poly(A) lengths from the same gene were distributed over a wide range (Supplementary Figure S1B; PAIsoSeq_Wu_2022.csv). Poly(A) spike-in molecules were used to verify the precise length of poly(A) (Supplementary Figure S1C). Initial observations suggested dynamic changes in the length and base composition of RNA tails.

In addition to poly(A) length measurements (20), we also performed mapping analysis from PAIso-seq data (Figure 1A). We defined the 3′ region of a transcript that could not be mapped to the genome as 'unmapped'. Almost all transcripts terminated with a poly(A) tract at the 3′ end, although the start site of the 3′-unmapped region was at times ambiguous. For example, the first adenosine could either be considered as the initiation of poly(A) or be mapped to a downstream position on the genome. These ambiguities were designated as mixed base addition (MBA) regions. In ∼97% (147 058) of transcripts, the ambiguous starting site was due to the assignment of adenosines to genomic or 3′-added sequence. Thus, the MBA region of these transcripts was part of the poly(A) region, having very short length (50th percentile = 1 and 75th percentile = 3) (Figure 1B, bottom; Supplementary Figure S1D), and most bases of the MBA region were adenosines (Figure 1C, right). We refer to this group of transcripts as poly(A) RNA (Figure 1D). In addition, a few (∼3%, 4665) transcripts had an MBA region that was neither mapped nor a part of poly(A) but was followed by poly(A) tails (Figure 1A, top). The MBA region in this group of transcripts was significantly longer (50th percentile = 3 and 75th percentile = 12) (Figure 1B, top) and dramatically enriched with uridine residues (Figure 1C, left). We designated this group of transcripts as uridylated-poly(A) or U-poly(A) RNA (Figure 1D; Supplementary Figure S1F).

To examine additional differences between poly(A) and uridylated-poly(A) transcripts, we profiled poly(A) lengths and read lengths. The uridylated-poly(A) transcripts had an increased number of short poly(A) transcripts and a slightly decreased number of long poly(A) transcripts (Figure 1E). The CCS read length of uridylated-poly(A) and poly(A) groups was almost identical (Supplementary Figure S1E). From the 9351 sequenced genes, 80% (7489) of genes had only poly(A) transcripts, which were defined as poly(A) genes. About 20% (1862) of genes had uridylated-poly(A) transcripts, including 2% (160) of genes that only had uridylated-poly(A) RNA and 18% (1702) of genes that had both types of transcripts (Figure 1F; Supplementary Figure S1F). Both groups (20%) were defined as uridylated-poly(A) genes. The PAIso-seq results were highly reproducible for each genotype (Figure 1G; Supplementary Figure S1G–K). Thus, using PAIso-seq analysis, we discovered the existence of a small cohort of uridylated-poly(A) transcripts in wild-type GV oocytes. Uridylated-poly(A) RNA was different from terminal uridylated transcripts because the polyuridine sequence was longer and the polyadenosine sequence occurred after the polyuridine sequence.

DIS3L2 depletion results in uridylated-poly(A) RNA accumulation and developmental arrest of oocytes

Cytoplasmic DIS3L2 ribonuclease is responsible for degrading terminally uridylated transcripts, and its depletion can cause transcriptome dysregulation in many cells (5,9). Transcripts of *Dis3l2* decreased during oocyte maturation (Supplementary Figure S2A) (4). Studies perturbing uridylyltransferases TUT4 and TUT7 indicated that uridylation and degradation of RNA occur extensively in maturing oocytes (15), and we hypothesized that DIS3L2 depletion would interfere with the degradation of specific transcripts. To test this hypothesis, we established *Dis3l2* floxed mice and crossed them with *Zp3-cre* mice to ablate *Dis3l2* in growing oocytes (Figure 2A; Supplementary Figure S2B). The resultant female mice ($Dis3l2^{cKO}$) were infertile (Figure 2B). Ovaries from $Dis3l2^{cKO}$ females had normal morphology and weight, and folliculogenesis was appropriately induced by hormone stimulation (Supplementary Figure S2C-E), suggesting unaffected oocyte growth. The diameter of $Dis3l2^{cKO}$ GV oocytes was comparable with that of controls (Supplementary Figure S2F). However, most $Dis3l2^{cKO}$ oocytes arrested at the GV stage without undergoing nuclear envelope breakdown or completing meiosis (Figure 2C, D). Depletion of *Dis3l2* transcripts was confirmed by qPCR in growing and fully grown GV oocytes (Figure 2E). The nuclear configuration remained normal since the ratio between surrounded nucleolus (SN) and non-surrounded nucleolus (NSN) oocytes was similar to that of control oocytes (Figure 2F). Microinjection of synthesized *Dis3l2-mVenus* RNA could not rescue the GV arrest of $Dis3l2^{cKO}$ oocytes, suggesting that the DIS3L2 depletion may result in additional or earlier changes (Supplementary Figure S2G). In summary, depletion of DIS3L2 caused oocyte arrest at the GV stage.

Using PAIso-seq, we analyzed transcripts from $Dis3l2^{cKO}$ oocytes that were comparable in number with control (Ctrl) oocytes (120 803 versus 151 723) and mapped to an equivalent number of genes (10 068 versus 9351). The overall distribution of poly(A) length in $Dis3l2^{cKO}$ oocytes was similar to that in controls except for a shift toward shorter poly(A) lengths (Figure 2G). As many as 37% (44 471) were uridylated-poly(A) transcripts (compared with 3% in controls), whereas only 63% (76 332) were poly(A) transcripts (Figure 2H). The shorter poly(A) length of uridylated-poly(A) transcripts was accentuated in $Dis3l2^{cKO}$ oocytes (Figure 2I). Sequence analysis indicated a striking increase in length of the MBA region in uridylated-poly(A) RNA; with a median value of 24 nt (Figure 2J; Supplementary Figure S3A, I). As expected, a dramati-

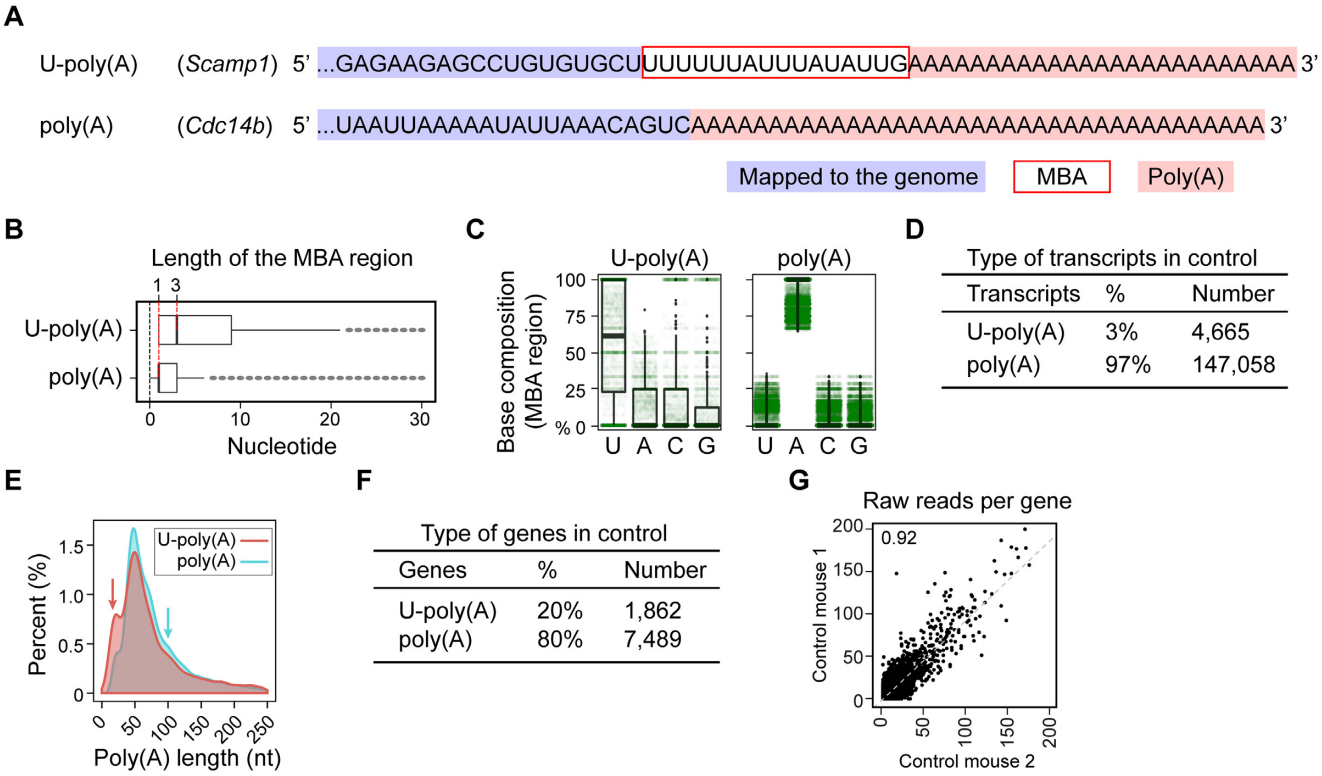

Figure 1. Uridylated-poly(A) RNA exists in GV oocytes. (**A**) Examples of uridylated-poly(A) RNA (*Scamp1*) and poly(A) RNA (*Cdc14b*) from PAIso-seq of wild-type (Ctrl) oocytes. Each transcript is analyzed by poly(A) measurement and alignment-based mapping. The light blue and light red backgrounds label the mapped region and the identified poly(A) region. The solid red box highlights the mixed base addition (MBA) region which is the ambiguous starting site of the 3′-unmapped region of some transcripts. (**B**) Boxplot showing the length of the MBA region in uridylated-poly(A) RNA and poly(A) RNA (nt). Each box shows the 25%, median and 75% of the MBA region length. The red dashed lines label the median length values in poly(A) RNA (1 nt) and uridylated-poly(A) RNA (3 nt). The outliers having MBA length >30 are not included, which comprise fewer than 5% of all transcripts. (**C**) Boxplot showing the percentage of U, A, C and G in the MBA region in uridylated-poly(A) RNA and poly(A) RNA. The transcripts that have an MBA region length of 0 are not included. (**D**) The number and percentage of uridylated-poly(A) RNAs and poly(A) RNAs in control oocytes. (**E**) Distribution of the poly(A) length of uridylated-poly(A) RNA and poly(A) RNA. Arrows indicate the left shift of the red line. (**F**) The number and percentage of genes that have uridylated-poly(A) RNA and poly(A) RNA. Note that uridylated-poly(A) genes may also have poly(A) transcripts, while poly(A) genes only have poly(A) transcripts. (**G**) Linear regression analysis between read number per gene in two biological replicates (two different control mice). Oocytes from the same mouse are pooled together. The number indicates the coefficient of correlation. Each dot is one gene. The *x*- and *y*-axes are the number of transcripts from this gene in mouse 1 and mouse 2.

cally high percentage of uridine was observed in the MBA region in uridylated-poly(A) transcripts (Figure 2K; Supplementary Figure S3B). When mapped to genes, 75% (7530) of genes had uridylated-poly(A) RNA, including 27% (2700) of genes that had only uridylated-poly(A) transcripts and 48% (4830) of genes that had both uridylated-poly(A) and poly(A) transcripts (Figure 2L; Supplementary Figure S3C, D). There were 2538 (25%) genes that only had poly(A) transcripts compared with 80% in the control (Figure 2L). We observed a significant shift of RNA from poly(A) to uridylated-poly(A) pools. About 83% of genes (1542/1862) that originally had uridylated-poly(A) RNA in control oocytes continued to have uridylated-poly(A) RNA in *Dis3l2*^{cKO} oocytes but significantly increased the ratio of uridylated-poly(A) versus poly(A) transcripts (Figure 2M; Supplementary Table S1). In addition, there were 5988 genes that did not have uridylated-poly(A) transcripts in controls but gained *de novo* uridylated-poly(A) transcripts in *Dis3l2*^{cKO} oocytes (Supplementary Table S1). Thus, *Dis3l2*^{cKO} oocytes had a 9.5-fold increase (44 471/4665) of uridylated-poly(A) transcripts (Figures 1D and 2H). The number of genes with associated uridylated-poly(A) RNA increased 4-fold (7530/1862) (Figures 1F and 2L; Supplementary Figure S3E–H).

To validate the apparent generation of the uridylated-poly(A) RNA, we synthesized *mVenus* mRNA without polyadenylation and microinjected it into oocytes. In control oocytes, we observed a short oligo(U) at the 3′ terminus, whereas in the *Dis3l2*^{cKO} oocytes, we observed a much longer string of uridines followed by polyadenylation (Figure 2N). We also performed validation of endogenous genes using Sanger sequencing by both PAIso-seq and a 3′-end ligation method to capture RNAs independent of poly(A). As an example, *H1f1* mRNA contained both uridylated-poly(A) and terminally truncated transcripts (Figure 2O; Supplementary Figure S3J). These results validated our PAIso-seq observations that uridylated-poly(A) transcripts can be generated from uridylated RNAs in *Dis3l2*^{cKO} oocytes. In summary, DIS3L2 ribonuclease depletion dramatically stabilized uridylated-poly(A) transcripts which then become prominent in the transcriptome.

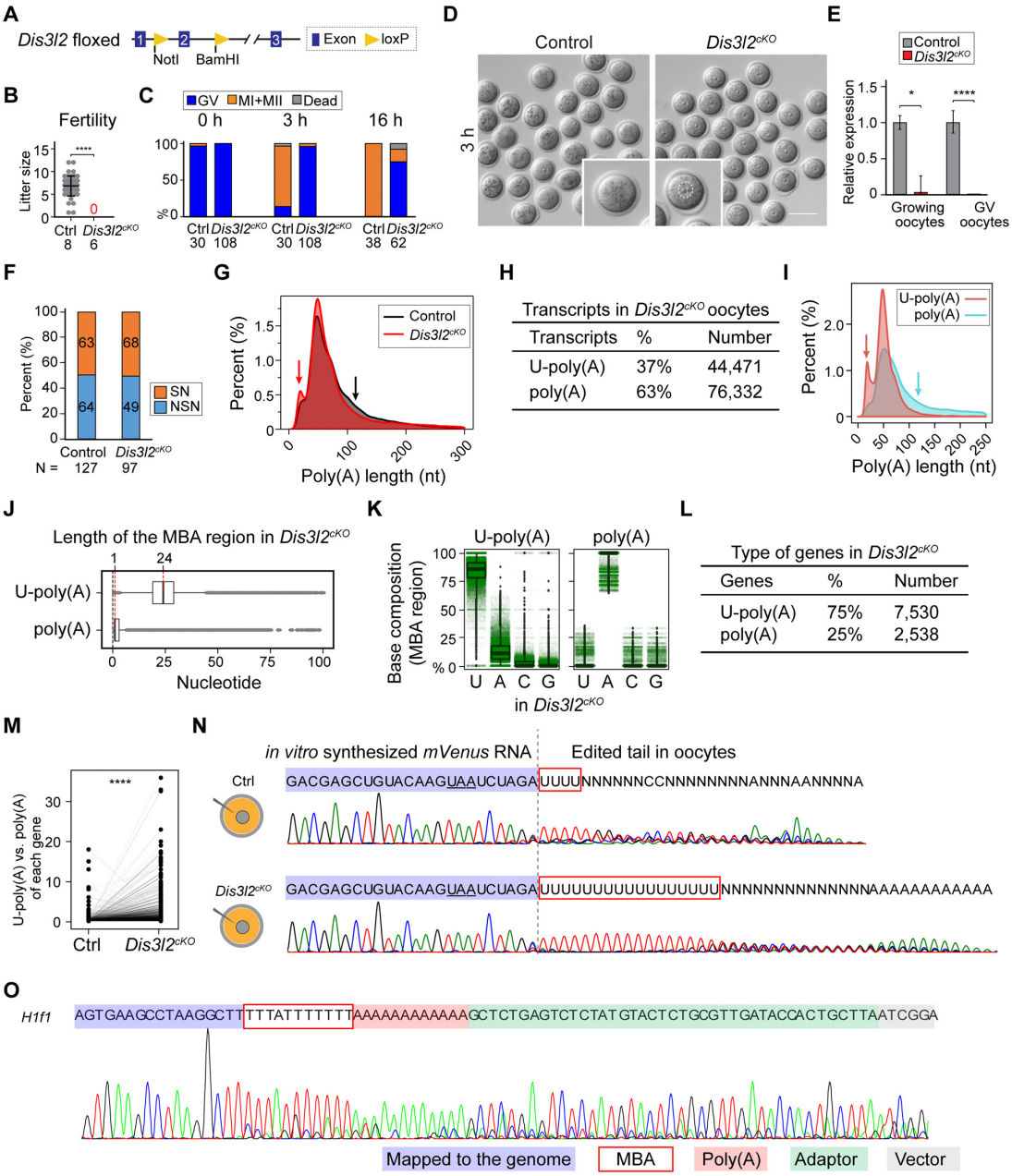

Figure 2. DIS3L2 genetic depletion stabilizes uridylated-poly(A) RNA. (**A**) Schematic of the floxed allele of the *Dis3l2* gene. Two loxP sites are inserted surrounding exon 2 using CRISPR/Cas9. (**B**) Dot plot showing the litter size of control and *Dis3l2*^{cKO} female mice of 6-month-old harem breeders. The number of females is labeled below each group. Note that none of the *Dis3l2*^{cKO} female mice had a litter. (**C**) *Ex vivo* culture of the GV oocytes at 0, 3 and 16 h. The number of oocytes is labeled below each group and is combined from three independent assays. (**D**) Live imaging of GV oocytes after 3 h *ex vivo* culture. Inset shows an individual oocyte magnified 2×. The white dashed circle labels the intact nuclear envelope in *Dis3l2*^{cKO} oocytes which breaks down in control oocytes. Scale bar, 100 μm. (**E**) qPCR validation of *Dis3l2* transcripts in growing oocytes (70 μm diameter obtained from P20 females) and fully grown GV oocytes. *0.04, ****4.06e-07. (**F**) Bar graph showing the percentage of surrounded nucleolus (SN) and non-surrounded nucleolus (NSN) oocytes in control and *Dis3l2*^{cKO} oocytes. (**G**) Density plot showing the distribution of transcripts of different poly(A) lengths in control and *Dis3l2*^{cKO} oocytes. Arrows indicate the left shift of the red line. (**H**) The number and percentage of uridylated-poly(A) RNA and poly(A) RNA in *Dis3l2*^{cKO} oocytes. (**I**) Distribution of the poly(A) length of uridylated-poly(A) RNA and poly(A) RNA in *Dis3l2*^{cKO} oocytes. Arrows indicate the left shift of the red line. (**J**) Boxplot showing the length of the MBA region of uridylated-poly(A) RNA and poly(A) RNA (nt) in *Dis3l2*^{cKO} oocytes. The red dashed lines label the median values in poly(A) RNA (1 nt) and uridylated-poly(A) RNA (24 nt). The outliers having MBA length >100 nt (<5% of all transcripts) are not included. (**K**) Boxplot showing the base composition in the MBA region in uridylated-poly(A) RNA and poly(A) RNA in *Dis3l2*^{cKO} oocytes. (**L**) The number and percentage of uridylated-poly(A) genes and poly(A) genes in *Dis3l2*^{cKO} oocytes. (**M**) The ratio between uridylated-poly(A) RNA and poly(A) RNA of the 1542 genes that have both uridylated-poly(A) RNA and poly(A) RNA in control and *Dis3l2*^{cKO} oocytes. ****6.60E-62, one-way ANOVA test. (**N**) *In vitro* synthesized *mVenus* mRNA was microinjected into either control or *Dis3l2*^{cKO} oocytes, purified, adaptor ligated, amplified and sequenced. The blue background indicates the *mVenus* coding region up to the stop codon (UAA, underlined). Placement of the restriction enzyme site (XbaI, TCTAGA) ensures the end of the DNA template after which RNA polymerase disengages during *in vitro* RNA synthesis. (**O**) PCR validation of individual genes from PAIso-seq results. As an example, the *H1f1* transcript is amplified for Sanger sequencing. The mapped coding region, MBA region, poly(A) region, adaptor and vector regions are indicated.

Uridylated-poly(A) RNA in *Dis3l2*^{cKO} oocytes globally stabilizes the transcriptome

Transcriptome analysis during meiotic maturation of *Dis3l2*^{cKO} oocytes documented perturbation in the transition from GV to meiosis II (MII) stages (Supplementary Figure S4A, left). Because of the overall poly(A) length shift and the potential tail disruption of transcripts in *Dis3l2*^{cKO} oocytes, we performed single-oocyte RNA-seq using both poly(A)-based and non-poly(A) based (rRNA depletion from total RNA, termed RiboMinus RNA-seq) methods. The dominance of uridylated-poly(A) RNA predicted a divergence between the two technologies, and we observed significantly greater abundance of transcripts in RiboMinus RNA-seq (Figure 3A, B; Supplementary Tables S2 and S3). We then aligned the spike-in (ERCC)-normalized counts of genes sequenced by the two methods and confirmed this discrepancy (Figure 3C). The RiboMinus preference suggested that many RNAs having increased abundance were not captured by poly(A) RNA-seq. In both methods, the *Dis3l2*^{cKO} oocytes contained more uridylated-poly(A) genes than control oocytes (Figure 3D).

Next, we categorized genes into down-regulated (Dn), unchanged (Un) and up-regulated (Up) groups according to the differential analysis results of RiboMinus RNA-seq. In each group, the numbers of poly(A) transcripts and uridylated-poly(A) transcripts were quantified in control and *Dis3l2*^{cKO} oocytes. The uridylated-poly(A) transcripts had the highest percentage in the Up group in *Dis3l2*^{cKO} oocytes, which is consistent with our previous findings of shorter poly(A) in *Dis3l2*^{cKO} oocytes (Figure 3E and F; Supplementary Figure S4C).

Due to limitations of poly(A)-mediated capture of transcripts in PAIso-seq, we could not detect reads that have extremely short or absent poly(A) tails. We sought to determine possible accumulation of uridylated transcripts in *Dis3l2*^{cKO} oocytes by identifying up-regulated genes that were specific to only one RNA-seq method and plotting their poly(A) length (Figure 3G). The 5370 up-regulated genes specific to the RiboMinus RNA-seq [i.e. not up-regulated in poly(A) RNA-seq] decreased their poly(A) length upon DIS3L2 depletion, whereas the 26 up-regulated genes specific to the poly(A) RNA-seq (i.e. not up-regulated in RiboMinus RNA-seq) increased their poly(A) length upon DIS3L2 depletion (Figure 3H, I). In addition, when we compared our PAIso-seq results with published TAIL-seq (15), we found that TAIL-seq detected 12 941 genes from mouse GV oocytes, which was 28.5% (2873 genes) more than the number of genes detected in our PAIso-seq (10 068 genes). The genes undetected by PAIso-seq may lack poly(A) tails in their transcripts.

We also performed more integrated analyses of RNA-seq and PAIso-seq in which we quantified the percentage of uridylated-poly(A) transcripts in individual *Dis3l2*^{cKO} oocyte having >1000 CCS reads. As a result, *Dis3l2*^{cKO} oocytes had a dramatic increase in uridylated-poly(A) RNA (Figure 3J). When we extracted the top 100 genes contributing to most changes between control and *Dis3l2*^{cKO} oocytes through principal component analysis of RiboMinus RNA-seq data, 57 genes were detected in PAIso-seq (Supplementary Figure S4A, B). Almost all genes had increased abundance (normalized by total CCS reads number) in *Dis3l2*^{cKO} oocytes (Figure 3K). Among all the transcripts belonging to the 57 genes, the number of poly(A) RNAs increased by 2.5-fold, while the number of uridylated-poly(A) RNAs increased by 100-fold (Figure 3L), which confirms the increase of uridylated-poly(A) RNA globally.

We then explored the differentially expressed genes for the biological mechanism of the GV arrest by DIS3L2 depletion. Among all the genes that could be detected by both methods, we paid special attention to the 823 genes that had increased abundance in both RNA-seq methods, which represented genes normally degraded but which were readenylated instead. Many genes encoded transcription factors, histone components and cell cycle regulators (Figure 3M; Supplementary Table S4). *Wee1*, a gene that inhibits meiotic progression, was also up-regulated, and had a substantial increase of uridylated-poly(A) transcripts (Figure 3N; Supplementary Figure S4D). WEE1's downstream effector, phosphorylated CDK1$^{Thr14, Tyr15}$ that represses GV oocytes from resuming meiosis, persists in *Dis3l2*^{cKO} oocytes at the GV 3 h stage (Figure 3O). To conclude, the transition of poly(A) to uridylated-poly(A) transcripts due to DIS3L2 ribonuclease depletion results in global stabilization of mRNAs including repressor proteins for meiotic progression, which may contribute to meiotic arrest observed in *Dis3l2*^{cKO} oocytes.

Uridylated-poly(A) RNA uses regular polyadenylation sites at the 3′ end

To examine the sequence integrity of uridylated-poly(A) RNA, we performed coverage profiling of reads from both RiboMinus RNA-seq and PAIso-seq. The RiboMinus RNA-seq data provided more unbiased capture of the transcriptome due to random priming during library construction whereas PAIso-seq exhibited a strong 3′ bias due to poly(A)-based capturing. As a result, we did not observe an obvious shift in read coverage in *Dis3l2*^{cKO} oocytes, suggesting that the integrity of most transcripts was not compromised by DIS3L2 depletion (Figure 4A, B).

We then employed the TAPAS algorithm to detect polyadenylation sites in the sequencing reads (26) and aligned the positions of the detected polyadenylation sites of each gene from control and *Dis3l2*^{cKO} oocytes. The polyadenylation sites aligned very well for most genes, suggesting that their transcripts had normal integrity and used the same polyadenylation sites in *Dis3l2*^{cKO} and control oocytes (Figure 4C). The numbers of polyadenylation sites detected in control and *Dis3l2*^{cKO} oocytes were similar (59.4% of genes/79.2% of transcripts in control, 47.6% of genes/71.1% of transcripts in *Dis3l2*^{cKO} oocytes) (Figure 4D, E). To further examine the polyadenylation sites, we selected seven oocyte-specific genes to plot their 3′-UTR length, which was the position of the 3′-unmapped region relative to the stop codon of the corresponding gene. Some genes contained a portion of irregular polyadenylation sites which was probably due to partial degradation (Figure 4F). Nevertheless, for most transcripts, the positions exhibited highly similar patterns in *Dis3l2*^{cKO} and control oocytes,

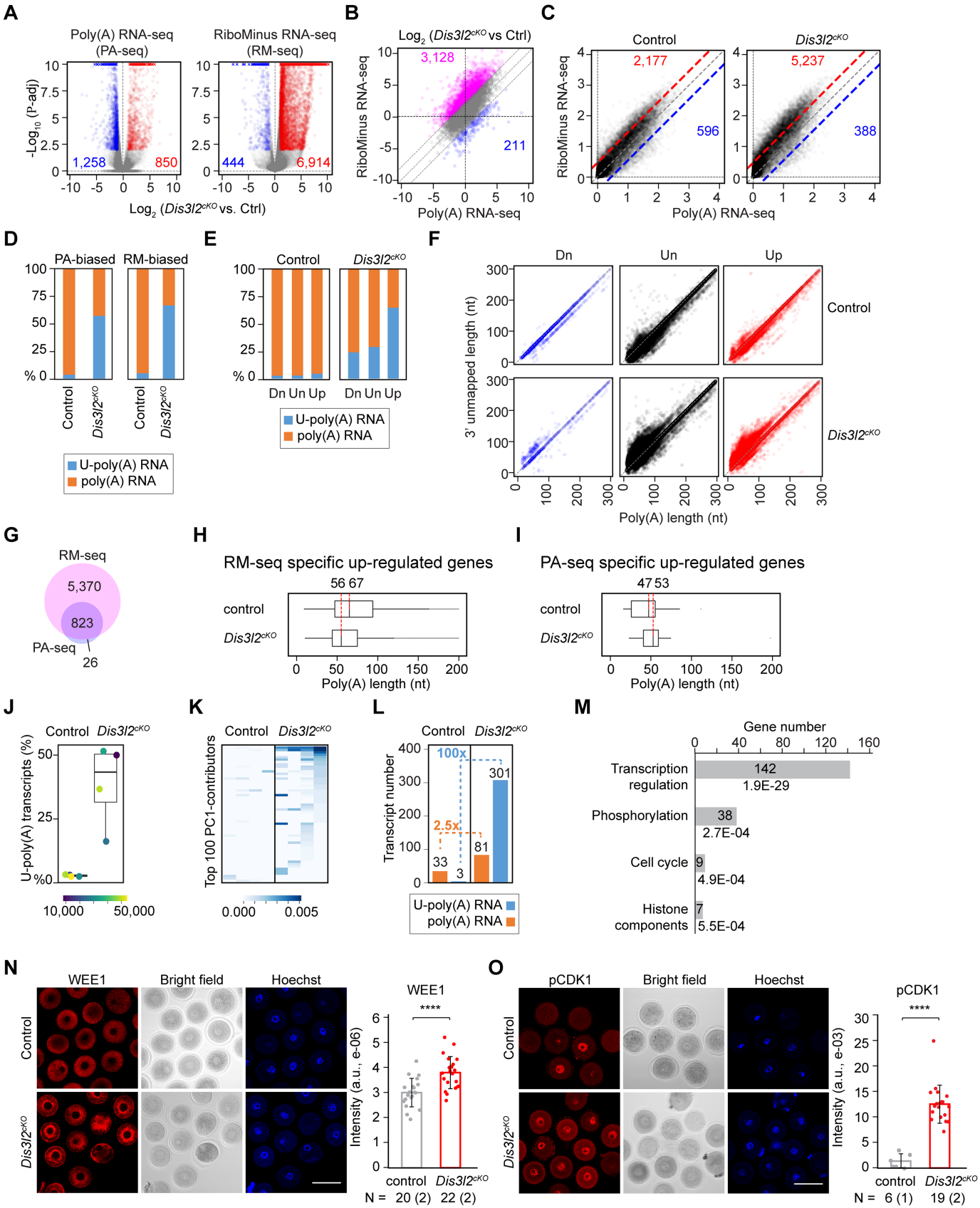

Figure 3. Accumulation of short poly(A) transcripts in *Dis3l2*^{cKO} oocytes. (**A**) Volcano plots showing differentially expressed genes detected from single-oocyte poly(A) RNA-seq and total RNA by selectively depleting rRNA (RiboMinus) RNA-seq. Red dots label transcripts with increased abundance and

suggesting that most transcripts used the same polyadenylation sites (Figure 4F).

Uridylated-poly(A) RNA has lower translation in *Dis3l2*^{cKO} oocytes

To examine the stability and translation of uridylated-poly(A) RNA, we engineered *mVenus* mRNA to have different tail sequences and included polyadenylated *mCherry* mRNA as a microinjection control (Figure 5A). Because RNAs with or without poly(A) have different capture efficiencies and amplification rates using different methods, we established four qPCR strategies for determining the stability of *mVenus* RNA: (i) oligo(dT)-based reverse transcription and amplification of the coding region; (ii) random hexamer-based reverse transcription and amplification of the coding regions; (iii) a gene-specific primer (GSP-1) that used a 3′-ligated adaptor for reverse transcription and amplification of the coding region; and (iv) a gene-specific primer (GSP-2), that used a 3′-ligated adaptor for reverse transcription and amplification of the 3′ end (Supplementary Figure S5A).

We tested *mVenus* mRNA with or without poly(A) to quantify and compare the different assays (Supplementary Figure S5B, C) and determined that random primers documented higher stability of *mVenus*-poly(A) compared with *mVenus* alone. GSP-2 did not detect *mVenus*-poly(A) due to the known attenuation of PCR efficiency for enriched regions of adenosine, and GSP-2 worked most efficiently when mRNA had short poly(A) (Supplementary Figure S5D, E). We observed an increased level of *mVenus* in *Dis3l2*^{cKO} oocytes, which suggested that deadenylated mRNA was stabilized by DIS3L2 ribonuclease depletion (Figure 5B). Next, we tested *mVenus*-U(25) mRNA and observed higher stability in *Dis3l2*^{cKO} oocytes which indicated insufficient degradation of terminal uridylated transcripts. Interestingly, the addition of a canonical poly(A) signal, AAUAAA, further improved the stability of the mRNA [*mVenus*-AAUAAA-U(25)] (Figure 5B).

To examine the stability of uridylated-poly(A) RNA, we *in vitro* synthesized *mVenus*-U(25)-poly(A) and *mVenus*-AAUAAA-U(25)-poly(A). Overall, we observed stabilized uridylated-poly(A) RNA in *Dis3l2*^{cKO} oocytes (Figure 5C; Supplementary Figure S5E). The addition of AAUAAA modestly improved the stability of *mVenus*-U(25)-poly(A) in *Dis3l2*^{cKO} oocytes (Figure 5C). Thus, the uridylated-poly(A) RNA was unstable and underwent active clearance in control oocytes but could be stabilized upon DIS3L2 ribonuclease depletion.

Given the link between tail dynamics and translation, we sought to analyze protein expression of the synthesized mRNAs (Figure 5D, E; Supplementary Figure S5F). We used the mCherry signal as a reference for each experimental condition. Consistent with mRNA stability, the translation signal of *mVenus*, *mVenus*-U(25) and *mVenus*-AAUAAA-U(25) was almost undetectable. On the other hand, we consistently observed a slight decrease in translation of uridylated-poly(A) mRNA in *Dis3l2*^{cKO} compared with control oocytes (Figure 5E). We did not compare different isoforms of *mVenus* because of a potential systemic difference generated from the mRNA preparation, concentration measurement and dilution. The subtle changes in fluorescence may not outcompete the systemic difference unless the differences are very significant. In addition, the overall translation efficiency in *Dis3l2*^{cKO} oocytes was equivalent to that of control oocytes presumably due to increased abundance of mRNA that offsets decreased translation (Figure 5F). To conclude, uridylated-poly(A) RNAs could still translate, albeit less robustly, which was compensated by stabilization of their transcripts in *Dis3l2*^{cKO} oocytes.

Poly(A) RNA converts to uridylated-poly(A) RNA by insufficient degradation and active tail editing

We were interested in the biological process generating uridylated-poly(A) RNA. It is known that TUT4/7-mediated oligo-uridylation labels RNA for degradation in

←

blue dots label transcripts with decreased abundance in *Dis3l2*^{cKO} compared with control oocytes. The numbers of increased and decreased transcripts in each method are labeled in red and blue, respectively. Threshold of significance is $\log_2$ value as 1 or –1, *P*-adj as 0.01. (**B**) Dot plot showing correlation between differentially expressed transcripts detected in poly(A) RNA-seq and RiboMinus RNA-seq. The *x*-axis shows the $\log_2$ values of *Dis3l2*^{cKO} versus control from the poly(A) RNA-seq method; the *y*-axis shows $\log_2$ values of *Dis3l2*^{cKO} versus control from the RiboMinus RNA-seq. Dashed lines: $y = x$, $y = x + 2$ and $y = x - 2$, which define the poly(A)-biased genes (blue) and RiboMinus-biased genes (red). (**C**) Dot plot showing the correlation between the ERCC-normalized raw counts ($\log_{10}$ transformed) from poly(A) RNA-seq and RiboMinus RNA-seq in control (left) and *Dis3l2*^{cKO} (right) oocytes. The three dashed lines are $y = x$, $y = x + 0.46$ and $y = x - 0.46$, which define the poly(A)-biased (blue) and RiboMinus-biased (red) transcripts. The number of dots between the blue and the red lines are 95% of all transcripts. The number of biased transcripts is labeled in blue and red. (**D**) Percentage of poly(A) and uridylated-poly(A) RNA in control and in *Dis3l2*^{cKO} oocytes from poly(A) RNA-seq and RiboMinus RNA-seq. (**E**) Percentage of poly(A) and uridylated-poly(A) RNA in control (left) and in *Dis3l2*^{cKO} (right) oocytes. Transcripts are clustered as down-regulated (Dn), unchanged (Un) and up-regulated (Up) using RiboMinus RNA-seq. (**F**) Dot plots showing the tail length and poly(A) length of genes. Transcripts are clustered into down-regulated (Dn), unchanged (Un) and up-regulated (Up) according to RiboMinus RNA-seq results. (**G**) Venn diagram showing the number of up-regulated transcripts from poly(A) RNA-seq (PA) and RiboMinus RNA-seq (RM). There are 823 transcripts having increased abundance from the two methods. (**H** and **I**) Box plots showing the distribution of poly(A) length of RiboMinus RNA-seq (RM specific) up-regulated and poly(A) RNA-seq (PA specific) up-regulated transcripts. (**J**) Boxplot showing the percentage of uridylated-poly(A) transcripts in PAIso-seq libraries of control and *Dis3l2*^{cKO} oocytes. The dot color represents the number of CCS reads in each library. Libraries having >1000 CCS reads are shown in the plot. (**K**) Heatmap showing the counts of 57 genes from PAIso-seq normalized by the CCS read number of each library. The 57 genes are from the top 100 contributors of principal component 1 comprising the major changes in *Dis3l2*^{cKO} versus control in RiboMinus RNA-seq. Columns are libraries containing >1000 CCS reads. (**L**) Bar plot showing the transcript number of uridylated-poly(A) RNA and poly(A) RNA in the 57 genes from (K). The number of poly(A) RNA increases 2.5-fold from control to *Dis3l2*^{cKO} oocytes, whereas the number of uridylated-poly(A) RNA increases 100-fold. (**M**) Functional enrichment of the 823 up-regulated transcripts that are shared between PA and RM. The number of genes enriched in each term and the *P*-value are labeled. (**N** and **O**) Confocal microscopy and quantification of immunostaining of WEE1 at the GV stage (N) and pCDK1 (Thr14, Tyr15) at the GV 3 h stage (O). The number of oocytes and mice is labeled below each bar. **** in WEE1, 0.0001, **** in pCDK1, 3.57e-10. The group picture represents one of three biological replicates.

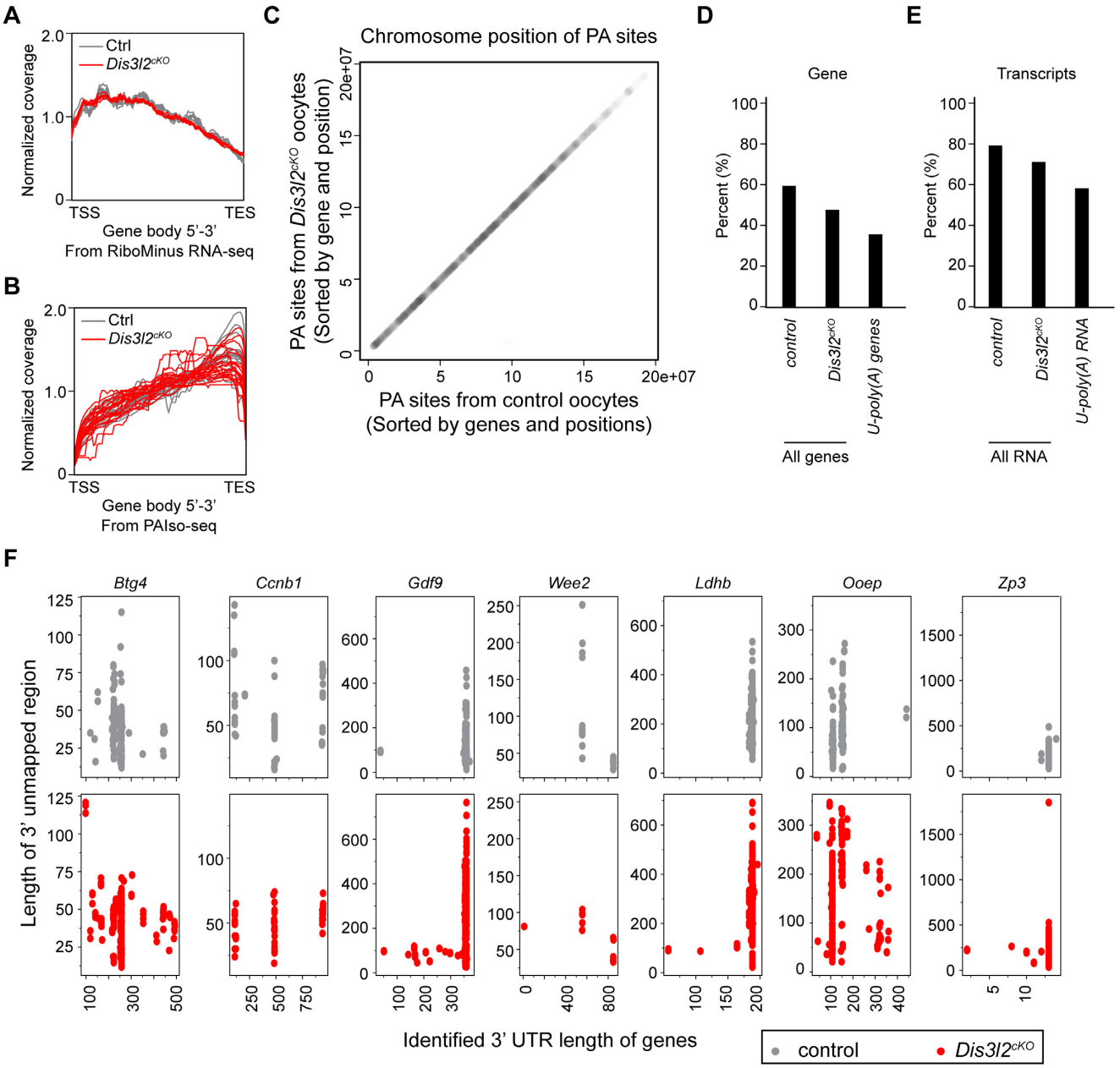

Figure 4. Uridylated-poly(A) RNA uses similar polyadenylation signals to poly(A) RNA and exhibits modest 3′ UTR loss**.** (**A** and **B**) Read coverage analyzed from RiboMinus RNA-seq (A) and PAIso-seq (B). TSS, transcription start site; TES, transcription end site. Reads are normalized by sequencing depth. (**C**) Scatter plot showing the positions of the identified polyadenylation (PA) sites in control and *Dis3l2*^{cKO} PAIso-seq samples. Each dot is a gene, the *x* and *y* are the positions of PA sites on chromosomes. Most genes have only one identified PA site. For genes with more than one PA site, the sites are sorted before being plotted. (**D** and **E**) Percentage of genes (D) and transcripts (E) that have one or more identified PA sites from PAIso-seq. The U-poly(A) genes and transcripts are calculated separately in addition to all genes/transcripts. (**F**) Plots of the 3′-unmapped region length of seven example genes in control and *Dis3l2*^{cKO} based on PAIso-seq results. Each dot is one 3′-unmapped region extracted from one read in PAIso-seq. The *x*-axis indicates the start position of this 3′-unmapped region relative to the translation end site (TAA) of the gene. A cluster of dots at the same 3′-UTR position indicates a conventional polyadenylation signal site.

oocytes. Thus, we hypothesized that the increased abundance of uridylated-poly(A) RNA came from RNAs that failed to undergo degradation after terminal uridylation. To test this, we analyzed the uridylated-poly(A) and poly(A) RNA composition of the up-regulated genes reported after TUT4/7 depletion (15). Indeed, for the 661 genes that were stabilized by TUT4/7 depletion, 402 were detected by PAIso-seq of control oocytes and 83 genes (20%) had uridylated-poly(A) transcripts, whereas 523 were detected in *Dis3l2*^{cKO} oocytes and 501 genes (96%) had uridylated-poly(A) transcripts (Figure 6A). In addition, upon DIS3L2 depletion, the genes stabilized by TUT4/7 depletion had a higher percentage of uridylated-poly(A) genes than those not up-regulated by TUT4/7 depletion (Figure 6A). These observations suggest that TUT4/7-uridylated transcripts labeled for degradation were able to be readenylated. How-

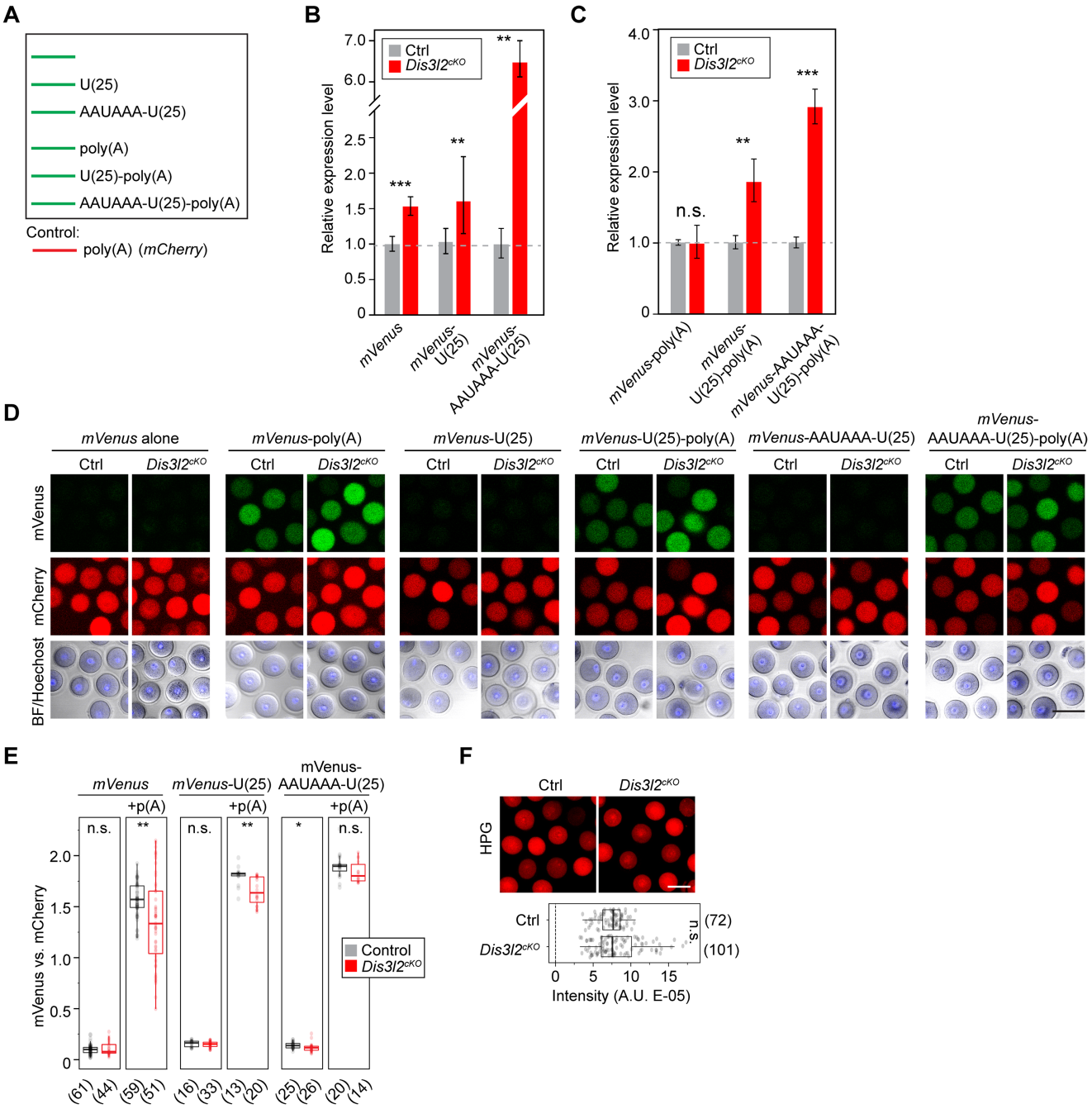

Figure 5. Uridylated-poly(A) RNAs are stabilized and have lower translation in *Dis3l2*^{cKO} oocytes. (**A**) Schematics of *in vitro* synthesized *mVenus* mRNA with different tails, namely *mVenus*, *mVenus*-U(25), *mVenus*-AAUAAA-U(25), *mVenus*-poly(A), *mVenus*-U(25)-poly(A) and *mVenus*-AAUAAA-U(25)-poly(A). Between *mVenus* and U(25), and between AAUAAA and U(25), there is an N15 spacer of 15 random bases (see the Materials and Methods). Each engineered *mVenus* mRNA was mixed with *mCherry*-poly(A) mRNA as an injection control. (**B**) Bar graphs showing the relative expression of *mVenus, mVenus*-U(25) and *mVenus*-AAUAAA-U(25) in control and *Dis3l2*^{cKO} oocytes. qPCR with random primers was used to determine the levels of *mVenus* normalized to co-injected *mCherry*. (**C**) Bar graphs showing the relative expression level of polyadenylated RNA, including *mVenus-poly*(A), *mVenus*-U(25)-poly(A) and *mVenus*-AAUAAA-U(25)-poly(A). The levels of *mVenus*-U(25)-poly(A) and *mVenus*-AAUAAA-U(25)-poly(A) are relative to *mVenus*-poly(A) in control and in *Dis3l2*^{cKO} oocytes, respectively. $^{**}P$ <0.01, $^{***}P$ <0.001, n.s., not significant. (**D**) Fluorescence images of oocytes, including mVenus, mCherry and merged bright field and Hoechst (BF/Hoechst). (**E**) Normalized fluorescence intensity of mVenus translated from differently engineered *mVenus* mRNAs. Results are two independent assays combined. The number of oocytes is labeled below each group. n.s., not significant; ** in *mVenus*-poly(A), $P = 0.002$; ** in *mVenus*-U(25)-poly(A), $P = 0.0012$; * in *mVenus*-AAUAAA-U(25)-poly(A), $P = 0.02$. (**F**) HPG labeling of translation activity and quantification. The number of oocytes is labeled next to each group. Scale bars: 100 μm.

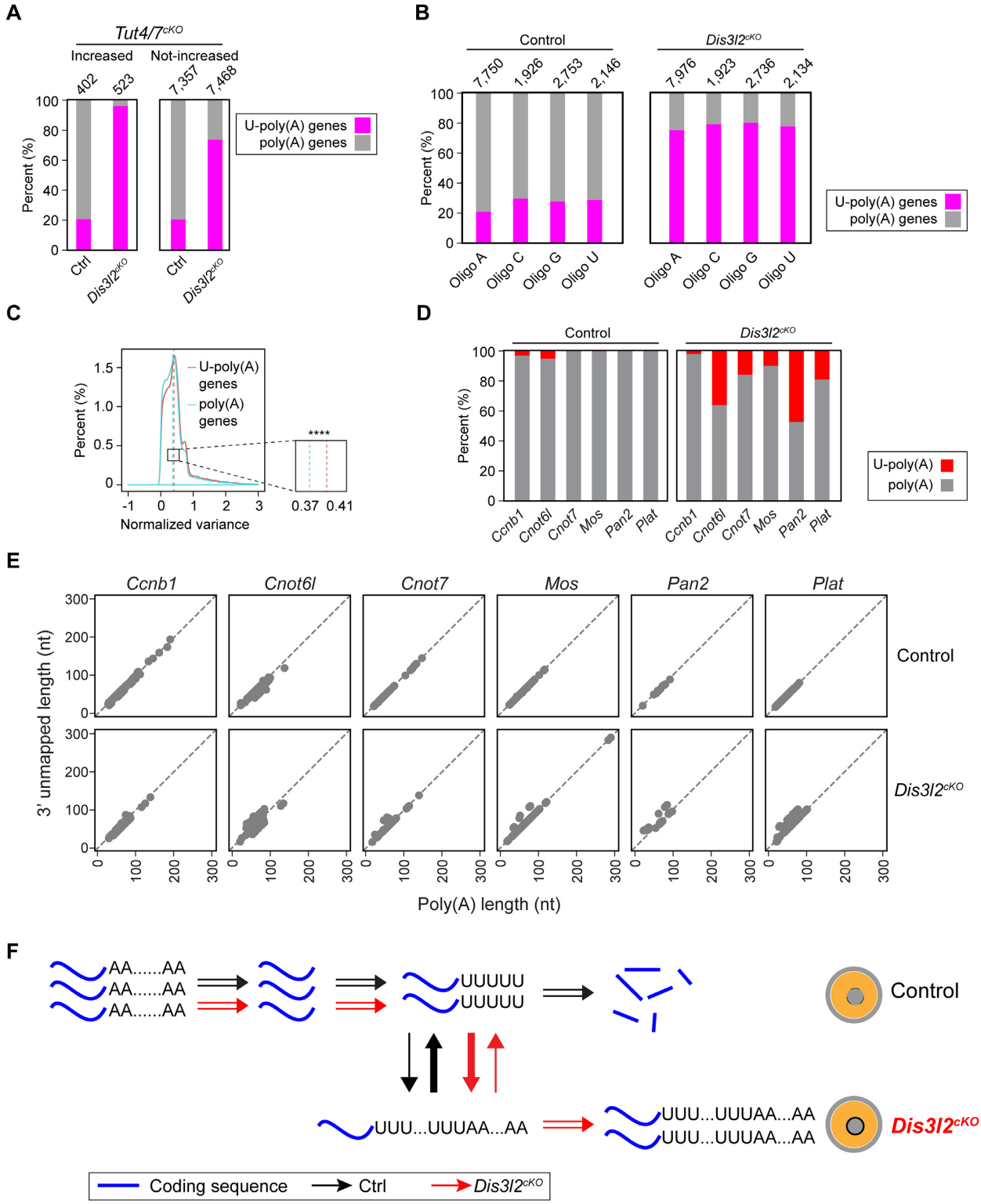

Figure 6. Active tail editing drives uridylated-poly(A) generation from poly(A) RNA. (**A**) Percentage of uridylated-poly(A) and poly(A) transcripts in control and *Dis3l2*^{cKO} oocytes. Transcripts are clustered as increased or not increased in *Tut4/7*^{cKO} oocytes. The number of transcripts is labeled above each group. (**B**) Percentage of uridylated-poly(A) and poly(A) genes. Genes are clustered as oligo A, oligo C, oligo G and oligo U terminally modified. The number of genes is labeled above each group. (**C**) Distribution of the normalized poly(A) length variance of uridylated-poly(A) and poly(A) transcripts. ****5.46e-16, *F*-test. (**D**) Percentage of uridylated-poly(A) RNA and poly(A) RNA in each of six dormant genes in mouse oocytes in control and *Dis3l2*^{cKO} oocytes. (**E**) Dot plots showing the 3′-unmapped region length and poly(A) length of the six dormant genes in control and *Dis3l2*^{cKO} oocytes. (**F**) Model of RNA degradation and tail editing that regulate RNA transiting between poly(A), uridylated and uridylated-poly(A) status. The uridylated-poly(A) RNA is quickly degraded by DIS3L2 ribonuclease. Upon genetic depletion of DIS3L2, uridylated RNA is poorly degraded, which results in global accumulation of uridylated-poly(A) RNA.

ever, when we compared genes having uridylated-poly(A) or poly(A) RNA with the list of genes that have terminal modifications in GV oocytes, we noted that genes with terminal uridylation contained a similar percentage of uridylated-poly(A) RNA compared with genes having terminal A/C/G-modified RNA (Figure 6B). This suggests that terminal uridylation may not be sufficient to cause uridylated-poly(A) formation. We also explored whether the read coverage in PAIso-seq could affect the percentage of uridylated-poly(A) RNA. We categorized the genes into extremely low (only one read), low (2–10 reads), mid (10–50 reads) and high (>50 reads), and plotted the uridylated-poly(A) RNA and poly(A) RNA for each group. As a result, the low-count genes had a higher ratio of uridylated-poly(A) RNA than high-count genes (Supplementary Figure S5G, H). We reasoned that the low-count genes were more likely to contain transcripts undergoing degradation, which were stabilized in *Dis3l2*^{cKO} oocytes. Nevertheless, we did not observe any bias of their terminal modification from TAIL-seq (Supplementary Figure S5H) (15). Thus, we conclude that some uridylated-poly(A) transcripts may be derived from transcripts other than the residual uridylated transcripts that failed to be degraded.

We next investigated if uridylated-poly(A) RNA was generated by tail editing including de- and readenylation. In this scenario, transcripts that could form uridylated-poly(A) RNA in control oocytes should have higher tail editing activities than the transcripts that could not form uridylated-poly(A) RNA. We employed normalized variance to represent the tail length dynamics and calculated its distribution in the two cohorts. As predicted, transcripts which contained uridylated-poly(A) RNA had a greater distribution of poly(A) length compared with those that did not contain uridylated-poly(A) (Figure 6C).

In mammalian oocytes, dormant mRNA persists during oogenesis and is not translated into protein until oocyte maturation. According to our model, transcripts of dormant mRNA were predicted to have uridylated-poly(A) RNA due to their highly dynamic tails. We then profiled the tails of known dormant RNAs, including *Ccnb1*, *Cnot6l*, *Cnot7*, *Mos*, *Pan2* and *Plat* (1,16,18). All gained uridylated-poly(A) transcripts upon DIS3L2 ribonuclease depletion (Figure 6D, E). Thus, at least a portion of uridylated-poly(A) RNA generated from poly(A) RNA is due to active tail editing.

To conclude, we discovered a small percentage of transcripts having uridylated-poly(A) in their 3′ termini. The low level of uridylated-poly(A) RNA is maintained by DIS3L2 ribonuclease, whose depletion results in accumulation of uridylated-poly(A) RNA in the transcriptome. The uridylated-poly(A) RNA was generated not only by insufficient degradation of uridylated RNA, but also from robust RNA tail editing (Figure 6F).

DISCUSSION

mRNA tail dynamics determine the stability of transcripts and their translation into protein. Using PAIso-seq, we discovered a small population of uridylated-poly(A) mRNA in mouse GV oocytes. The existence of uridylated-poly(A) RNAs has been reported recently (28), but their biological significance remains unclear. Production of uridylated-poly(A) RNA is post-transcriptional, non-templated and dynamic. The fate of uridylated transcripts is not preordained but is modulated by tail editing for either readenylation or degradation. Upon genetic depletion of DIS3L2 ribonuclease, many poly(A) mRNAs are transformed into uridylated-poly(A) mRNAs which are more stable, and this results in global accumulation of transcripts. In general, those transcripts destined for conversion into uridylated-poly(A) mRNA have greater 3′ tail editing. Our findings add a novel mode to mRNA tail regulation in maturing mouse oocytes in which readenylation occurs after uridylation. We propose that DIS3L2 ribonuclease functions as an RNA quality gatekeeper to prevent the accumulation of uridylated transcripts and their readenylated products.

From TAIL-seq analysis, terminal oligo uridylation is often fewer than five residues (15). Because capture of RNA in PAIso-seq depends on the 3′ poly(A) sequence, we were not able to isolate transcripts when they have uridine at the 3′ termini. As a result, we did not observe the accumulation of terminal uridylated transcripts after DIS3L2 ribonuclease depletion. We performed several analyses to indirectly address this point: (i) comparison of the tail sequence using RiboMinus RNA-seq and poly(A) RNA-seq; (ii) evaluation of poly(A) length of transcripts that are specifically up-regulated in each RNA-seq method; and (iii) comparing the number of detected genes in PAIso-seq with published TAIL-seq data. By incorporating gene counts in the detection of uridylated-poly(A) RNA, we further observed a higher occurrence of uridylated-poly(A) RNA in low-count genes, which may be due to the active degradation of these mRNAs under normal conditions and suggests the absence of poly(A) or truncated transcripts. It is possible that transcripts without poly(A) exist in *Dis3l2*^{cKO} oocytes and escape detection. However, uridylated-poly(A) RNA can explain ∼60% of the RiboMinus RNA-seq increase of transcript abundance (Figure 3), and we conclude that increased uridylated-poly(A) RNA is at least one of the major biological changes caused by DIS3L2 ribonuclease depletion. Our results also indicate that TUT4/7 uridylation may potentially elongate (from <5 to ∼24 nt) if not recognized and degraded by DIS3L2. Thus, under wild-type conditions, TUT4/7-mediated uridylation and DIS3L2-mediated degradation are tightly coupled to promptly limit the presence of uridylated-poly(A) RNA transcripts.

RNA stability and translation involve both 5′ and 3′ regulation (29). The 5′ cap of the mRNA not only mediates formation of the translation initiation complex, but also regulates the 5′ RNA degradation machinery. Deadenylated RNAs are substrates for both 3′ degradation and 5′ decapping/degradation. In our PAIso-seq result, we were not able to analyze the 5′ coverage due to the 3′ bias of this method. However, the read length and the 5′ coverage by RiboMinus RNA-seq did not significantly change after DIS3L2 depletion, which suggests intact activity of the 5′ RNA degradation. In addition, transcripts in *Dis3l2*^{cKO} oocytes mostly use the same polyadenylation signal sequences as control oocytes, suggesting that most reads have integrity, and tail edits occur in the 3′-UTR. We also observed increased stability and reduced translation of the uridylated-poly(A) RNA in *Dis3l2*^{cKO} compared

with control oocytes. We reason that these readenylated transcripts could recruit poly(A)-binding proteins to maintain the eIF4F complex and mRNA cap integrity required for translation (30). However, the length of the poly(A) tails of the uridylated-poly(A) RNA became shorter which may perturb recruitment of poly(A)-binding proteins and compromise initiation of translation. In turn, decreased translation may lower the stability of uridylated-poly(A) RNA compared with poly(A) RNA. Other than the features of the transcripts, the global translation activity of DIS3L2-depleted oocytes also may be compromised due to translation machinery proteins that have been insufficiently translated. Overall, in *Dis3l2*^{cKO} oocytes, uridylated-poly(A) RNAs are stabilized due to insufficient degradation and tail editing.

When looking into the dysregulated functional genes, we identified several meiotic regulatory genes, including *Rad21l*, *Meioc*, *Nr2c2*, *Sycp3* and *Tubgcp6*, some of which have known meiosis-related promoting or repressive roles (31–33). The accumulated uridylated-poly(A) RNAs and their compromised translation make it hard to predict the protein level of these genes. We reason that elimination of repressive RNA is critical to foster resumption of meiosis. Thus, when transcripts of inhibitory genes accumulate, such as *Wee1*, the persistent cognate protein may be more likely to cause arrest of oocytes by, in this example, activating the meiotic repressor pCDK1. In addition, oocyte depletion of DIS3L2 exhibits a more severe and much earlier arrest in transitioning from meiosis I prophase to metaphase, compared with the *Tut4/7*^{cKO} oocytes that have spindle defects in meiosis I anaphase to telophase (15). This suggests that DIS3L2 also has TUT4/7-independent functions in licensing resumption of meiosis.

During oocyte development, tail editing could happen earlier than the GV stage, e.g. during the oocyte growth phase. Both *Dis3l2*^{cKO} and *Tut4/7*^{cKO} oocytes employ *Zp3-cre* to delete the genes in growing oocytes and result in the GV arrest phenotype. *Dis3l2*^{cKO} GV oocytes are morphologically normal, but there may be some early-changed transcripts plus secondary effects which together cause the unsuccessful rescue by overexpressing *Dis3l2* mRNA at the GV stage.

To conclude, during mouse oocyte development, uridylated-poly(A) RNA is actively generated from both uridylation-labeled RNA degradation and tail editing. After DIS3L2 depletion, many transcripts accumulate and are transformed into uridylated-poly(A) RNA which results in global transcriptome stabilization. The insufficient degradation of meiotic repressor transcripts may cause the GV arrest of *Dis3l2*^{cKO} oocytes. Normally, DIS3L2 degrades uridylated transcripts to ensure meiotic resumption of mouse oocytes necessary for female fertility.

DATA AVAILABILITY

All the sequencing analysis codes are available at https://github.com/Di-aswater/public-dis3l2-analysis. Raw and processed files are in GSE208531.

SUPPLEMENTARY DATA

Supplementary Data are available at NAR Online.

ACKNOWLEDGEMENTS

We are grateful for the useful discussions from colleagues in the Dean lab at the NIDDK, LCDB, especially Dr Guanghui Yang and Dr Ye Yang. We are also grateful for the discussions and suggestions from the bioinformatics core at the NIDDK, LCDB. We thank Dr Shaohe Wang, NIDCR, for the constructive help and tutorial in performing PAIso-seq mapping analysis, and Dr Yusheng Liu from the Institute of Genetics and Developmental Biology, Chinese Academy of Sciences for sharing the PAIso-seq protocol.

Author contributions: D.W. and J.D. conceived the project. D.W. designed the experiments and performed most of the experiments and analyses. M.P. established the PAIso-seq pipeline and imaged ovary histology. J.C. established and optimized the HPG labeling assay. D.W. organized figures and wrote the manuscript. M.P. wrote the manuscript. J.C. and J.D. edited the manuscript.

FUNDING

This work was supported by the National Institutes of Health [1ZIADK015603-15].

Conflict of interest statement. None declared.

REFERENCES

1. Sagata,N. (1996) Meiotic metaphase arrest in animal oocytes: its mechanisms and biological significance. *Trends Cell Biol.*, **6**, 22–28.
2. Von Stetina,J.R. and Orr-Weaver,T.L. (2011) Developmental control of oocyte maturation and egg activation in metazoan models. *Cold Spring Harb. Perspect. Biol.*, **3**, a005553.
3. Ma,J., Fukuda,Y. and Schultz,R.M. (2015) Mobilization of dormant Cnot7 mRNA promotes deadenylation of maternal transcripts during mouse oocyte maturation. *Biol. Reprod.*, **93**, 48.
4. Wu,D. and Dean,J. (2020) EXOSC10 sculpts the transcriptome during the growth-to-maturation transition in mouse oocytes. *Nucleic Acids Res.*, **48**, 5349–5365.
5. Astuti,D., Morris,M.R., Cooper,W.N., Staals,R.H., Wake,N.C., Fews,G.A., Gill,H., Gentle,D., Shuib,S., Ricketts,C.J. *et al.* (2012) Germline mutations in DIS3L2 cause the Perlman syndrome of overgrowth and Wilms tumor susceptibility. *Nat. Genet.*, **44**, 277–284.
6. Malecki,M., Viegas,S.C., Carneiro,T., Golik,P., Dressaire,C., Ferreira,M.G. and Arraiano,C.M. (2013) The exoribonuclease Dis3L2 defines a novel eukaryotic RNA degradation pathway. *EMBO J.*, **32**, 1842–1854.
7. Faehnle,C.R., Walleshauser,J. and Joshua-Tor,L. (2014) Mechanism of Dis3l2 substrate recognition in the Lin28–let-7 pathway. *Nature*, **514**, 252–256.
8. Ustianenko,D., Pasulka,J., Feketova,Z., Bednarik,L., Zigackova,D., Fortova,A., Zavolan,M. and Vanacova,S. (2016) TUT–DIS3L2 is a mammalian surveillance pathway for aberrant structured non-coding RNAs. *EMBO J.*, **35**, 2179–2191.
9. Towler,B.P., Pashler,A.L., Haime,H.J., Przybyl,K.M., Viegas,S.C., Matos,R.G., Morley,S.J., Arraiano,C.M. and Newbury,S.F. (2020) Dis3L2 regulates cell proliferation and tissue growth through a conserved mechanism. *PLoS Genet.*, **16**, e1009297.
10. Pirouz,M., Wang,C.H., Liu,Q., Ebrahimi,A.G., Shamsi,F., Tseng,Y.H. and Gregory,R.I. (2020) The Perlman syndrome DIS3L2 exoribonuclease safeguards endoplasmic reticulum-targeted mRNA translation and calcium ion homeostasis. *Nat. Commun.*, **11**, 2619.
11. Tian,B., Hu,J., Zhang,H. and Lutz,C.S. (2005) A large-scale analysis of mRNA polyadenylation of human and mouse genes. *Nucleic Acids Res.*, **33**, 201–212.
12. Xiang,K. and Bartel,D.P. (2021) The molecular basis of coupling between poly(A)-tail length and translational efficiency. *Elife*, **10**, e66493.

13. Lima,S.A., Chipman,L.B., Nicholson,A.L., Chen,Y.H., Yee,B.A., Yeo,G.W., Coller,J. and Pasquinelli,A.E. (2017) Short poly(A) tails are a conserved feature of highly expressed genes. *Nat. Struct. Mol. Biol.*, **24**, 1057–1063.
14. Jiang,J.C., Zhang,H., Cao,L.R., Dai,X.X., Zhao,L.W., Liu,H.B. and Fan,H.Y. (2021) Oocyte meiosis-coupled poly(A) polymerase alpha phosphorylation and activation trigger maternal mRNA translation in mice. *Nucleic Acids Res.*, **49**, 5867–5880.
15. Morgan,M., Much,C., DiGiacomo,M., Azzi,C., Ivanova,I., Vitsios,D.M., Pistolic,J., Collier,P., Moreira,P.N., Benes,V. *et al.* (2017) mRNA 3′ uridylation and poly(A) tail length sculpt the mammalian maternal transcriptome. *Nature*, **548**, 347–351.
16. Svoboda,P., Stein,P., Hayashi,H. and Schultz,R.M. (2000) Selective reduction of dormant maternal mRNAs in mouse oocytes by RNA interference. *Development*, **127**, 4147–4156.
17. Yu,C., Ji,S.Y., Sha,Q.Q., Dang,Y., Zhou,J.J., Zhang,Y.L., Liu,Y., Wang,Z.W., Hu,B., Sun,Q.Y. *et al.* (2016) BTG4 is a meiotic cell cycle-coupled maternal–zygotic-transition licensing factor in oocytes. *Nat. Struct. Mol. Biol.*, **23**, 387–394.
18. Kotani,T., Yasuda,K., Ota,R. and Yamashita,M. (2013) Cyclin B1 mRNA translation is temporally controlled through formation and disassembly of RNA granules. *J. Cell Biol.*, **202**, 1041–1055.
19. Yang,C.R., Rajkovic,G., Daldello,E.M., Luong,X.G., Chen,J. and Conti,M. (2020) The RNA-binding protein DAZL functions as repressor and activator of mRNA translation during oocyte maturation. *Nat. Commun.*, **11**, 1399.
20. Liu,Y., Nie,H., Liu,H. and Lu,F. (2019) Poly(A) inclusive RNA isoform sequencing (PAIso-seq) reveals wide-spread non-adenosine residues within RNA poly(A) tails. *Nat. Commun.*, **10**, 5292.
21. Hwang,W.Y., Fu,Y., Reyon,D., Maeder,M.L., Tsai,S.Q., Sander,J.D., Peterson,R.T., Yeh,J.R. and Joung,J.K. (2013) Efficient genome editing in zebrafish using a CRISPR-Cas system. *Nat. Biotechnol.*, **31**, 227–229.
22. de Vries,W.N., Binns,L.T., Fancher,K.S., Dean,J., Moore,R., Kemler,R. and Knowles,B.B. (2000) Expression of Cre recombinase in mouse oocytes: a means to study maternal effect genes. *Genesis*, **26**, 110–112.
23. Dobin,A., Davis,C.A., Schlesinger,F., Drenkow,J., Zaleski,C., Jha,S., Batut,P., Chaisson,M. and Gingeras,T.R. (2013) STAR: ultrafast universal RNA-seq aligner. *Bioinformatics*, **29**, 15–21.
24. Anders,S., Pyl,P.T. and Huber,W. (2015) HTSeq—a Python framework to work with high-throughput sequencing data. *Bioinformatics*, **31**, 166–169.
25. Love,M.I., Huber,W. and Anders,S. (2014) Moderated estimation of fold change and dispersion for RNA-seq data with DESeq2. *Genome Biol.*, **15**, 550.
26. Arefeen,A., Liu,J., Xiao,X. and Jiang,T. (2018) TAPAS: tool for alternative polyadenylation site analysis. *Bioinformatics*, **34**, 2521–2529.
27. Ramirez,F., Ryan,D.P., Gruning,B., Bhardwaj,V., Kilpert,F., Richter,A.S., Heyne,S., Dundar,F. and Manke,T. (2016) deepTools2: a next generation web server for deep-sequencing data analysis. *Nucleic Acids Res.*, **44**, W160–W165.
28. Liu,Y., Nie,H., Zhang,Y., Lu,F. and Wang,J. (2021) Comprehensive analysis of mRNA poly(A) tail reveals complex and conserved regulation. bioRxiv doi: https://doi.org/10.1101/2021.08.29.458068, 29 August 2021, preprint: not peer reviewed.
29. Franks,T.M. and Lykke-Andersen,J. (2008) The control of mRNA decapping and P-body formation. *Mol. Cell*, **32**, 605–615.
30. Brook,M., Smith,J.W. and Gray,N.K. (2009) The DAZL and PABP families: RNA-binding proteins with interrelated roles in translational control in oocytes. *Reproduction*, **137**, 595–617.
31. Herran,Y., Gutierrez-Caballero,C., Sanchez-Martin,M., Hernandez,T., Viera,A., Barbero,J.L., de Alava,E., de Rooij,D.G., Suja,J.A., Llano,E. *et al.* (2011) The cohesin subunit RAD21L functions in meiotic synapsis and exhibits sexual dimorphism in fertility. *EMBO J.*, **30**, 3091–3105.
32. Soh,Y.Q.S., Mikedis,M.M., Kojima,M., Godfrey,A.K., de Rooij,D.G. and Page,D.C. (2017) Meioc maintains an extended meiotic prophase I in mice. *PLoS Genet.*, **13**, e1006704.
33. Syrjanen,J.L., Pellegrini,L. and Davies,O.R. (2014) A molecular model for the role of SYCP3 in meiotic chromosome organisation. *Elife*, **3**, e02963.